Chinese Journal of Aeronautics 25 (2012) 189-197

Contents lists available at ScienceDirect

Chinese Journal of Aeronautics

journal homepage: www.elsevier.com/locate/cja

Large-scale Vacuum Vessel Design and Finite Element Analysis

WANG Wenlong, CAI Guobiao*, ZHOU Jianping

School of Astronautics, Beihang University, Beijing 100191, China

Received 26 April 2011; revised 24 October 2011; accepted 12 December 2011

Abstract

The vacuum plume effects experimental system (PES) is the first experimental system designed to study the effects of vacuum plume in China. The main equipment, a vacuum chamber of 5.5 m in diameter and 12.8 m in length, and structure design of hinged door are described. The finite element method (FEM) is adopted to analyze the static strength and stability of the PES vacuum chamber. It is demonstrated that the static strength and stability are qualified. For the 5.5 m diameter vacuum chamber door, three design schemes are put forward. After comparisons are made, the single-axis-double-pin hinged door is selected. The FEM is applied to checking its static strength as well as distortions. The results show that the door's distortion and displacement change mainly due to the gravity of the door which leads to its sinking. The calculated displacement is less than 7.8 mm, while the actual measurement is 5 mm. The single-axis-double-pin hinged door mechanism completely satisfies the design requirements. This innovative structure can be introduced as a reference for the design of large-scale hinged doors.

Keywords: vacuum; design; finite element method; buckling; chamber; hinges

1. Introduction

In the recent years, the vacuum plume effects of the thruster on board, such as additional forces and moments, excessive heat loads and contamination, have received considerable interest. Because of the great cost and time requirements associated with space-based experiments, ground-based experiment is necessary to compliment the limited data obtained in space. And the ground facilities must reproduce the space environment faithfully and consistently. Large-scale vacuum chamber plays an essential role in predicting the effects of vacuum plume. To meet the special requirements of the plume effect experiment, it is important to analyze the static strength and stability of vacuum chamber, as well as sealing performance [1-9].

The vacuum plume effects experiment system (PES), which is constructed in Beihang University, is not only the first test equipment for the study of plume effects in China but also the largest one in the world. The diameter of the main vacuum chamber is 5.5 m and the length of it is 12.8 m. Due to the special requirement of the cryopump's inlets and outlets and the parameter measurement of plume effects experiment, PES vacuum chamber belongs to particular equipment. There are totally 63 openings with various types, which are densely distributed on the body of vacuum chamber, so a scheme of wide span reinforcing rings is adopted firstly. The span of cabin is usually not larger than 1.5 m in congeneric chamber (∅ 5 m or larger). But in PES vacuum chamber, the maximum span of the reinforcing rings is 2.85 m and the minimum span is 1.68 m. As a typical welding structure of thick shell, PES vacuum chamber undergoes external pressure, so stress concentration and deflection, as well as instability, will take place in the region of openings [10-12]. Finite element method (FEM) is applied commonly to estimating the reliability and verifying the design of the chamber.

Due to the constraints of the space of testing hall and sealing performance of the door, the design of the opening type and mechanism of door is also difficult. The hinged door, with the advantage of space-saving,

*Corresponding author. Tel.: +86-10-82336533.
E-mail address: cgb@buaa.edu.cn
Foundation item: Ministry Level Project

doi: 10.1016/S1000-9361(11)60378-6

is the first choice. However, it is rarely adopted in region of large-scale chamber because of its fabrication and assembly deviation. The flange face of door cannot completely match the flange face of cabin, so the vacuum chamber cannot be sealed effectively. In addition, the long-term excessive load caused by the gravity distributed on hinges of the door will lead to the deformation between two faces aggravatingly. Moreover, shear stress on sealing ring will occur when closing the door forcibly. The sealing ring can be cut off quickly by the asymmetric force, which leads to degrading the performance of sealing ring intensively [13-17]. Based on the above reasons, side-open hinged door is replaced by translation-type or hanging-type door in congeneric chamber, which is designed and fabricated in the chambers of America, Europe and Japan. Although the hinged door has been adopted by a ∅5 m door of the space environment simulator (KM6) in China and a ∅7 m door in NASA, the problem of the sealing performance and deformation appear in long-term working [18].

In this paper, the static strength and the bulking of the chamber are carried out [10-11]. In addition, the discrepancy between the results of engineering experience formula and the FEA is discussed respectively. The original design, which takes the method of wide span reinforcing rings in multi-opening structure, is proved to be viable. Furthermore, three schemes of hinged structure by side open are proposed initially in this paper, which will be applied to the 5.5 m diameter door of the vacuum chamber. The details of the structures and advantage/disadvantage are presented, and the optimal scheme could be used to solve the question thoroughly and perfectly. The results of the deformation of the hinged door obtained by FEM and actual test are consistent. The sealing performance is satisfactory，which certificates that the analysis by FEM is reasonable.

2. Vacuum Chamber Design

2.1. Structure design of vacuum chamber

Because the volume pump rate is assumed to be 10^7 L/s or larger in vacuum plume effects experiment, a new total chamber pumping (TCP) concept is adopted to meet the requirement, i.e., the tube-plate area of liquid helium-driven fins must bigger than 240 m^2. In other words, the internal diameter of cabin and the length of chamber will not be less than 5.2 m and 12 m respectively, otherwise the tube-plate area cannot be reached. Based on the above reasons, the dimension of PES vacuum chamber is 5.5 m in diameter and 12.8 m in length, which is a cylindrical horizontal structure [2-9]. As illustrated in Fig. 1, the front and rear heads are standard elliptical shape, and two saddles are mounted at the bottom of the chamber. The stainless steel 0Cr18Ni9 and structural steel (16Mn or carbon steel) are used for cabin, heads, saddles and reinforcing rings respectively. The thicknesses of cabin and heads are both 18 mm. Owing to the special requirements of the heat sink entrance and exit, as well as the plume's experimental measurement, there are a total of 63 openings of various types in the vacuum vessel, with most of the openings being relatively dense. There are 38 openings, which include two 1 320 mm diameter openings of cryogenic pump flanges, four 400 mm diameter openings of viewing windows arranged symmetrically, and 32 measuring/spare openings on the plume vacuum chamber. There are 21 openings on rear head, which include one 320 mm diameter flange opening of roughing line and 20 flange openings of liquid nitrogen, liquid helium inlets and outlets for cryopump. There are four openings on the door, which include two inlets and two outlets flange openings of liquid nitrogen and liquid helium. According to Eq. (1), the nominal thickness of cabin is 13.4 mm.

$$\delta_{\mathrm{n}} = D_0\left(\frac{3pL_{\mathrm{c}}}{2.6ED_0}\right)^{0.4} + C \tag{1}$$

where δ_{n} represents the nominal thickness of cabin, p the atmospheric pressure, L_{c} the length of cabin, E elastic modulus, D_0 the diameter of the cabin, and C the additional value of the wall thickness.

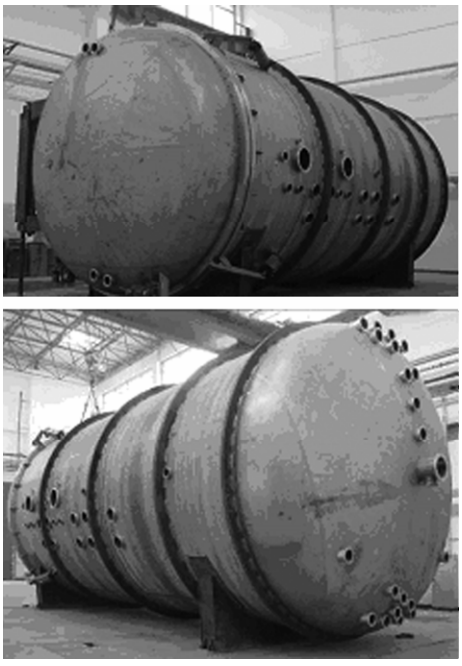

Fig. 1 Outside drawing of vacuum plume effect chamber.

Due to the specificity of the plume experiment and in order to meet the requirements of openings and the structural stability of the vessel, a scheme of large-scale span strengthening rings and concentrated openings is applied. The maximum span of the strengthening rings is 2 850 mm and the minimum span is 1 680 mm. The section of reinforcing rings is rectangle, 150 mm×100 mm. The material of the reinforcing rings is $45^{\#}$ carbon steel. The two heads of vacuum chamber is 2∶1 elliptic. According to Eq. (2), the nominal thickness of two

heads δ is 12.0 mm. However, considering the joint between heads and cabin and according to Eq. (2), the actual thickness of heads is 18 mm.

$$\delta = 3.2R_{\mathrm{i}}\sqrt{\frac{p}{E}} \tag{2}$$

where the variable R_{i} represents the internal diameter of the heads.

2.2. Structure of hinged door

In order to solve the problem of the improper fit of the door flange face and the cabin flange face, three schemes are proposed initially in the process of design of door, which include quasi-double hinged door mechanism, double-cylinder hinged door mechanism and single-axis-double-pin hinged door mechanism [14-16]. The weight of the door is 6 200 kg, the inner load of the door is about 1 500 kg in working condition, and the weight of hinged structure is about 2 000 kg. Since the hinged door is side-open, the stress of the hinged structure is asymmetric. All of the three schemes take the following assumption. The remote elastic support unit is set up at the bottom of the door, which will share the load of the gravity on the hinge; the position is 60° to the neutral surface of door. The support force is adjustable, and the range is from 10 kN to 30 kN. An elastic support at the bottom of hinged axis is mounted and the support force is the sum of the self-weight of the door, inner concentrated load and the self-weight of the hinges, which is used to share the load of the whole mechanism at the joint region of cabin.

2.2.1. Quasi-double hinged door mechanism

The structure of the quasi-double hinged door in Fig. 2 can be simplified as three linkage mechanisms, shown in Fig. 3. Due to the fabrication and assembly deviation, as well as the deformation caused by gravity, a flexible and restrictive switch device is adopted so as to avoid improper fit of the door flange face and the cabin flange face. Ideally, when the door is closed, the plane formed by two axles of hinges cannot be parallel with the central axis of the chamber (i.e. $\alpha \neq 0$). Otherwise, the phenomenon of "dead spots" will occur in rear axis. Suppose the rear axis can turn around of 360º, and the front axis is the restrictive axle, a geometric relationship can be gained from Fig. 3.

$$s = 2L\sin\left(\frac{\beta}{2}\right)\cos\left(\frac{\beta}{2}+\alpha\right) \tag{3}$$

where s represents the dislocation displacement of two faces of flanges, α and β are the restrictive rotating angles of the front and rear axes, and L is the length of the linkage. The dislocation displacement s would make the performance of sealing ring degenerate because of shear force, so the value of s should be close to 0. Obviously, when α=90º, the value of dislocation

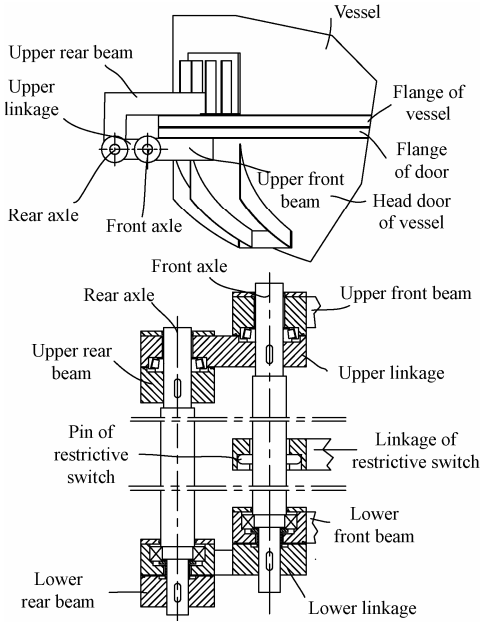

Fig. 2 Diagram of quasi-double hinged door mechanism.

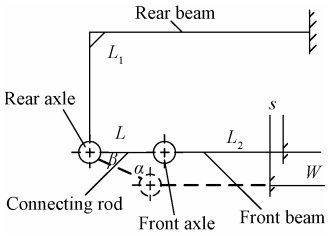

Fig. 3 Simplified diagram of quasi-double hinged door mechanism.

displacement is the minimum. That is to say, when the door is closed, the axis of rear linkage should coincide with the axis of front beam. The quasi-double hinged door mechanism should select rear axle as 360º axle. When the door is rotating, the steel frame plane composed of two front beams is on the same plane with the steel frame plane composed of two linkages, and the center of gravity of the door is also on the same plane. The structure is strengthened by steel frame, which is composed of two front beams and two linkages, and the force and torque caused by gravity of door on flanges can be decreased remarkably.

In fact, due to fabrication and assemble deflection, the mechanism will deviate from the theoretical design position as shown in Fig. 4(a). Thereby, when the door is closed, the flange face of the door will improperly fit with the flange face of cabin, which can be divided into two cases. When the rear axis is in the right side of the design position as shown in Fig. 4(b), after the door closes, there is a gap between the flange face of the door and the flange face of the cabin in the region near the hinges or remote side. In any of the two conditions, the problem of two flange faces not fitting with each other will be solved by means of fine-tuning the front beam clockwise or counterclockwise. When the rear axis is on the left side of the design position as shown

in Fig. 4(c), after the door closes, fine-tuning the linkages clockwise or counterclockwise can solve the problem in the same way.

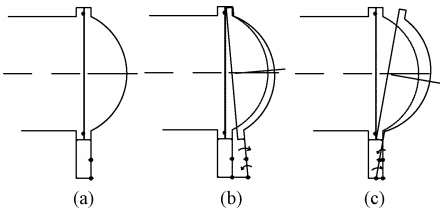

Fig. 4 Displacement compensation schematic diagram of quasi-double hinged door mechanism.

The restrictive rotating angle α of the front axis is related to the length L_2. By analyzing the geometric relationships, we can get $W=L_2 \sin \alpha$. In the equation, suppose α is constant, then the longer the front beam is, the larger the adjustable displacement is. Suppose L_2=150 mm. Since the adjustable displacement W is bigger than 10 mm,α cannot be smaller than 3.8º.

2.2.2. Double-cylinder hinged door mechanism

The dual-cylinder hinged door mechanism is shown in Fig. 5, the door can rotate around its axis of hinges. Due to gravity of the door, as well as the fact that the hinges are far from the center of gravity of the door, the load on the hinged door is complicated. The upper linkage is connected with the pull cylinder, while the lower linkage is connected with the push cylinder. The two linkages are installed on the two rear beams through their bearings respectively. There is an adjustable gap between linkages and rear beams. When the door is closed, once the two flange faces do not fit each other, the problem can be solved by means of pulling the cylinder to ensure that the linkages can move along axis direction of vacuum chamber.

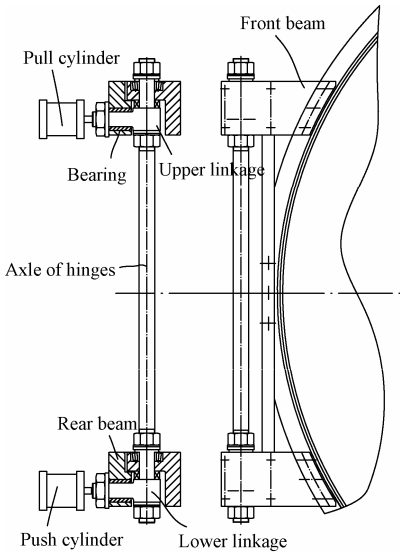

Fig. 5 Double-cylinder hinged door mechanism.

There is a push force on the lower linkage caused by the door rotating around the axis of hinges. In this condition, the adjustable gap along axis direction of vacuum chamber can be "eaten" by assembly deflection. A push cylinder is mounted on the other side of the lower linkage to eliminate the hidden trouble. As the door works, the push cylinder will resist the lower linkage so as to keep the adjustable gap from being "eaten".

While the door rotates around the axis, the upper linkage will slide in bearing. Because of asymmetric load, the "top death" problem between the linkage and bearing or between bearing and the rear beam, is inevitable. That trouble will induce the door not to work properly. To solve this problem, the linkages and bearing are lengthened. Meanwhile, another method by means of providing a pull force from the pulling cylinder along axis direction of linkages to avoid "top death" emerges. Three cylinders can work together to keep the door working healthily.

2.2.3. Single-axis-double-pin hinged door mechanism

The structure of double-cylinder hinged door mechanism is simple, but the working sequence of pushing or pulling cylinders is complicated. Additionally, the hidden trouble of bearing excessive stress is inevitable. Although the fine-tuning device can solve the problem of improper fit of the two flange faces of door and cabin, the joint region of hinges between the door and cabin is still on flanges, and it is indubitable to induce the stress concentration in the joint region. So it is necessary to strengthen the steel frame of hinges. In addition, the position of the center of gravity of the door locates outside the hinged mechanism, which is not conducive for the load of door, especially in the working condition of the door.

The single-axis-double-pin hinged door mechanism (as shown in Fig. 6) is improved on the basis of quasi-double hinged door mechanism. Both joints of the hinges, which are originally connected respectively with flange of cabin or flange of door, are changed to be connected with the head of the door or the body of the cabin. It is still necessary to strengthen the joint region, and it is especially important to make certain that the hinge mechanism and the center of gravity of

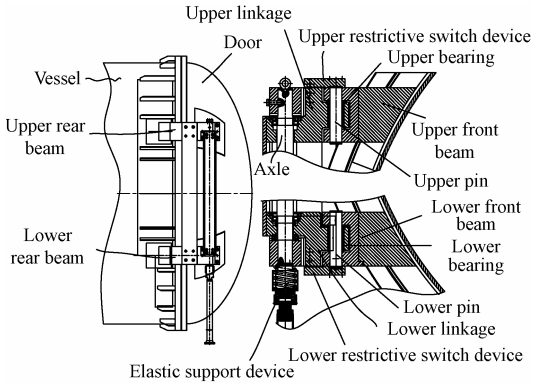

Fig. 6 Single-axis-double-pins hinged door mechanism.

door are on the same plane to eliminate torque. The restrictive switch device, as well as the double axes of quasi-double hinged door mechanism, is reserved, but the double axes is changed to a single axis and two pins [15-16].

3. Static Structural and Buckling Analysis

A 3D model for PES vacuum chamber is shown in Fig. 7. The 20-node entity mixed elements are used. Hexahedral mesh is adopted in the region of reinforcing rings and saddles, and tetrahedral mesh is applied in the rest of the region. It is necessary to encrypt the grid in the contact area and the transition domain. The saddles of vessel are made of carbon steel. The strengthening rings are made of 16Mn steel and the rest are of 0Cr18Ni9 stainless steel (For material parameters, see Table 1).

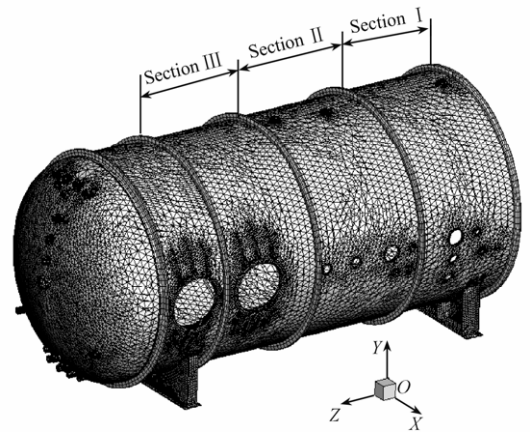

Fig. 7 Grid model of PES vacuum chamber.

Table 1 Material parameter

Material	Elastic modulus /GPa	Poisson ratio	Yield strength/ MPa	Density/ (kg·m^{-3})
Stainless steel	193	0.31	206.8	7 750
Carbon steel	210	0.30	220.6	7 850
16Mn	200	0.30	220.6	7 850
Bearing steel	210	0.28	620.4	7 700
Aluminum bronze	110	0.30	275.5	7 400

During calculations, the vacuum chamber is under gravity and the displacement of Y direction at the bottom surfaces of the two saddles is constrained. A standard atmospheric pressure on the external surface of vacuum chamber is applied. Meanwhile, the axial surface load on all faces of flanges is defined and the value of force is calculated according to Eq. (4).

$$F = p\frac{\pi D_{\mathrm{f}}^2}{4} \tag{4}$$

where D_{f} is the outside diameter of the flange [18-21].

The von Mises stress contour and the displacement contour of static strength analysis are respectively shown in Figs. 8-9. It can be seen from the figures that the average von Mises stress is less than 50 MPa, and the maximum von Mises stress is 96.8 MPa, which distributes in the contact region between cabin and saddles. The von Mises stress in the region of reinforcing rings is significantly smaller than the adjacent region, both of which are small enough not to break the structural strength. So the main purpose of reinforcing rings is to improve the stiffness of cabin. Different degrees of von Mises stress concentration appear in adjacent region of openings. The bigger the diameter of openings is, the more serious the degree is. Because of the reinforcing rings, the degree of stress concentration is decreased, especially in adjacent region of two openings of diameter 1 320 mm (illustrated in Fig. 8(a)). Without a reinforcing structure, the phenomenon of stress concentration at the adjacent region of flange 5.5 m in diameter of the door is obvious. However, the value of the von Mises stress is just about 60-70 MPa, which is still within the allowable range of material. Because the dimension of the outside contour of the chamber in radial direction is not continuous, a reinforcing structure is still adopted in adjacent region of flange of door to strengthen the local stiffness, shown in Fig. 1. For most of the openings, the effect of stress concentration is not obvious. So it is demonstrated that removing the reinforcing structure of openings, whose diameter is not bigger than 400 mm, is reasonable. Based on the above analysis, static strength of the whole vacuum chamber is qualified and the structure in the adjacent region of lacking of stiffness has been

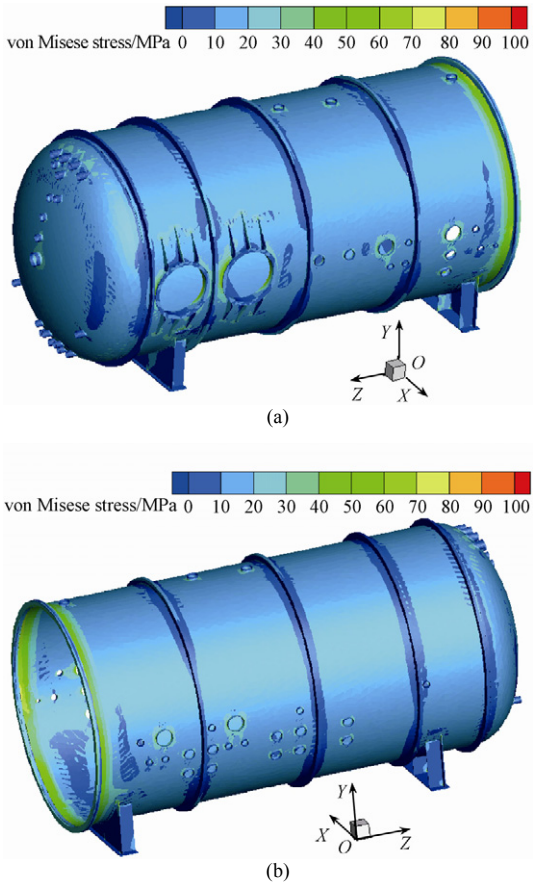

Fig. 8 von Mises stress contour of static strength.

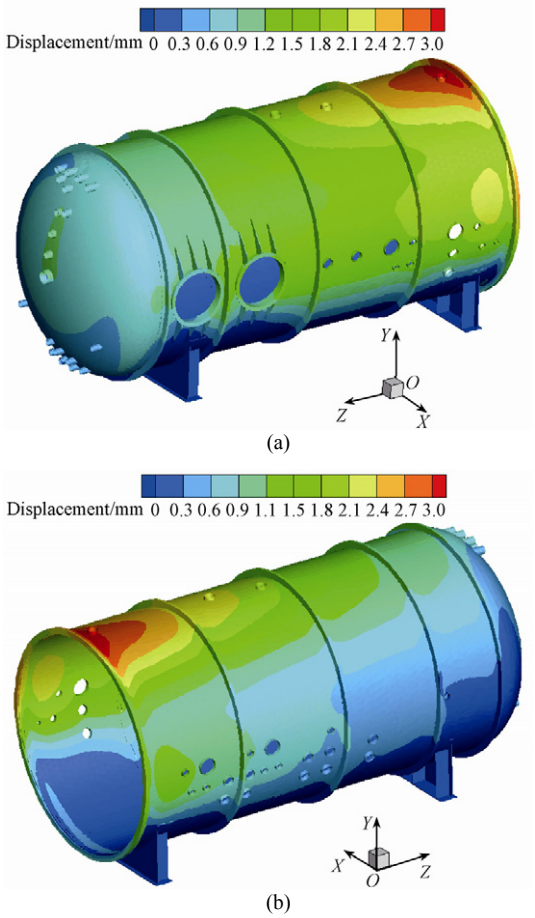

Fig. 9 Displacement contour of static strength analysis.

strengthened.

The maximum displacement of vacuum vessel is 3 mm, which occurs in the region of cabin and the top part of the vessel flange connection. This is because radial structure appears to be discontinuous in that region, which is the inevitable result of the horizontal vacuum vessel. Obviously, the deformation is not conducive to maintain the curvature of chamber flange. The deformation gradually decreases from the maximum displacement region in front flange of chamber to rear head of chamber and/or lower chamber direction, and reaches the minimum value 0 mm at the bottom plane of two saddles.

In buckling analysis, the load multiplier from the 1st to the 6th mode is calculated, as shown in Table 2. From the 1st mode to the 6th mode, the load multiplier increases. However, there is little difference between them or any obvious gradient as predicted. That is mainly because the PES vacuum chamber is a complex large-scale span reinforced composite shell. The span between any two reinforcing rings is different. So the load multiplier in every segment is different under the same mode. This can be verified by engineering experience Eq. (5),

$$P_{cr} = 2.6\frac{E\delta_e^2}{L_s D_0\sqrt{\dfrac{D_0}{\delta_e}}} \tag{5}$$

where P_{cr} is the critical pressure of instability, L_s the span between reinforcing rings, and δ_e the thickness of PES vacuum chamber. Table 3 is constructed by Eq. (5). It can be seen that at the same modal step, the load multiplier of each segment is different. This demonstrated that during buckling analysis, it is possible for load multiplier at each step to be close.

Table 2 Load multiplier for vacuum plume effect chamber buckling analysis with different modes

Mode	1	2	3	4	5	6
Load multiplier	8.17	8.19	8.49	8.51	8.86	8.99

Table 3 Lahm-equation calculation results of different L_s

L_s/mm	P_{cr}/MPa	Load multiplier
2 700	0.681 3	6.813
2 850	0.645 5	6.455
2 500	0.735 8	7.358
1 680	1.095 0	10.950

The deformation contour of vacuum chamber at the 1st mode is represented in Fig. 10. It can be seen that the maximum buckling occurs in Section II of the cabin, in which span is the largest. The critical load estimated from Eq. (5) is smaller than the characteristic value of FEM. That is because Eq. (5) simplifies calculation, without considering the influence of the structure strengthened at both heads in the calculation. No matter which calculation method is applied, when external pressure is smaller than 0.6 MPa, the chamber will not undergo instability.

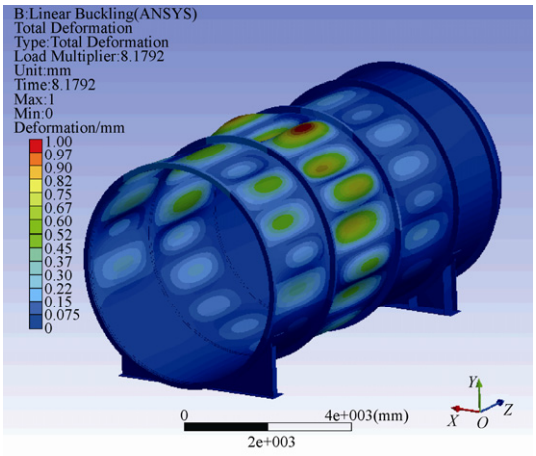

Fig. 10 Deformation contour at the 1st mode buckling analysis.

4. Static Strength Analysis of Single-axis-double-pin Hinged Door Mechanism

After comparison, the scheme of single-axis-double-pin hinged door mechanism is finally selected, and the static strength analysis of the single-axis-double-pin hinged door mechanism is completed [13, 18-19]. During the process of constructing the proportional three-di-

mensional geometric model, the restrictive switch device is removed, and single axis, double pins and other components are simplified, as shown in Fig. 11. The interaction between hinges and door/cabin is taken into account. A segment of cabin is constructed in the model and the length of the segment is bigger than the attenuation length of edge stress. The characteristic and parameters of all the materials are shown in Table 1. Two-order 10-node tetrahedron element is applied, which is based on the curvature parameter. It is indispensable to encrypt the grid at the region of contact area, as well as the transition domain. The displacement of X direction and Y direction is constrained on the plane of external section of cabin and the contact plane between cabin and saddle respectively. The gravity load on single-axis-double-pin hinged door mechanism is exerted. As much as 15 kN concentrated force is applied on the upper-inside of the door. The Case 1 is the condition without any load on the remote elastic support device or elastic support device. While the Case 2 is the condition which is loaded respectively with 10 kN and 80 kN on the bottom of remote elastic support device and the elastic support device.

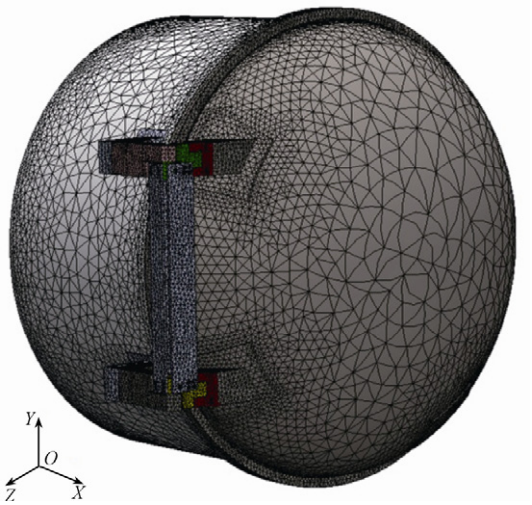

Fig. 11 Grid figure of single-axis-double-pins hinged door mechanism.

The von Mises stress contour in different conditions is shown in Fig. 12 and Fig. 13 respectively. The resultant displacement U_{res} contour of the two conditions is illustrated in Fig. 14 and Fig. 15 respectively. The displacement curve of the flange's outer edge is shown in Fig. 16. The von Mises stress concentration appears on the upper-inside of the door, which is caused by the 15 kN concentrated force. Another stress concentration appears in the region of the upper and lower rear beams. That is because of the pull force caused by gravity of door loading on the upper rear beam and push force loading on the lower rear beam. The maximum stress concentration exists in the region of lower rear beam, if the remote support device and the elastic support device are applied, which can share the load caused by gravity of the door on the upper and lower rear beams, then the value of von Mises stress decreases from 129.3 MPa to 63.1 MPa. Obviously, the two support devices can effectively alleviate the stress concentration. However, in the worst condition without any support device, the maximum von Mises stress of the mechanism still does not reach the yield stress of materials, and it is demonstrated that the static strength of the door mechanism is qualified.

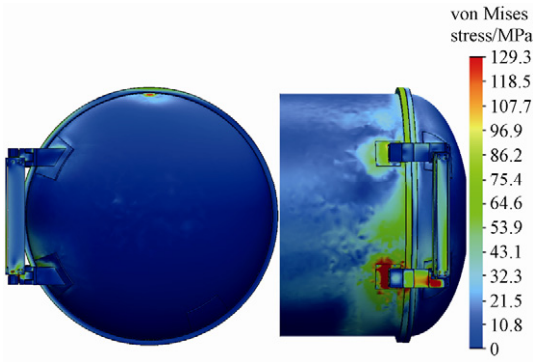

Fig. 12 von Mises stress contour of Case 1.

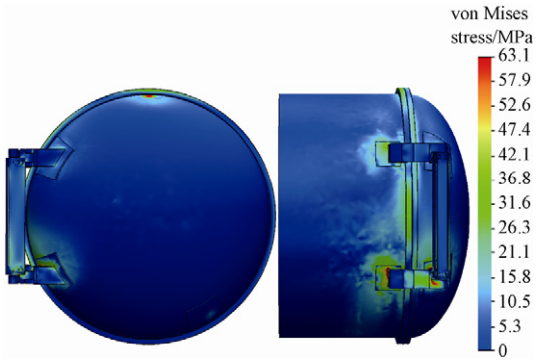

Fig. 13 von Mises stress contour of Case 2.

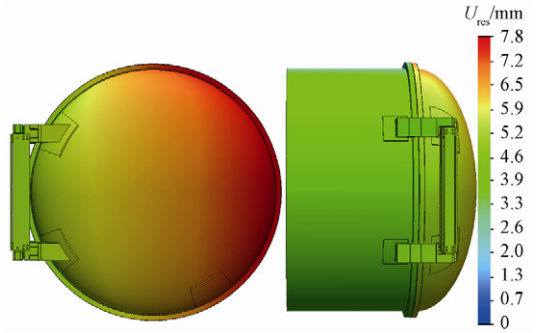

Fig. 14 The resultant displacement contour of Case 1.

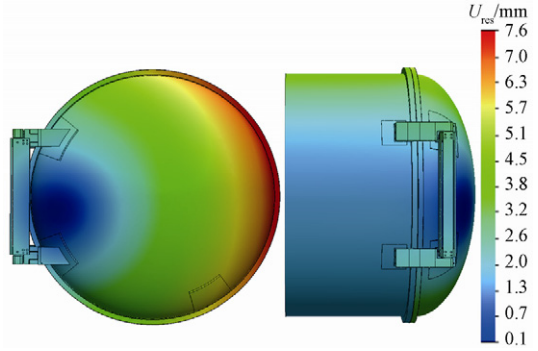

Fig. 15 The resultant displacement contour of Case 2.

As shown in Fig. 16, with the effect of the gravity of the door, a torque and warpage appear on the flange of door and head, which is caused by the reaction force from the upper and lower hinges. The displacement along the *X* direction and *Z* direction is caused by the torque and warpage, which occurs in the regions of upper and lower (90° and 270°) of the door flange's outside edge. The magnitude is equal but the direction is opposite. The displacement along *Z* direction is caused by pull force on the upper of flange and push force on the lower of flange, which are generated by mass force of the right side of door. In the range of 100º-280º, the deformation is remarkable, and on the right side of the flange of the door, the displacement reaches the largest value. The maximum value of displacement is 7.8 mm, which is mainly caused by the gravity of the door. The absolute displacement along *X* direction and *Z* direction is smaller than the value along *Y* direction. If the remote elastic support device and the elastic support device are applied, the resultant displacement decreases from 7.8 mm to 7.6 mm. The difference along *X* or *Y* direction is not obvious, however, the amplitude of displacement along *Z* direction is remarkable. That is because the balance between the force of 80 kN and 10 kN is broken, and a moment around the axis of the door appears. So, whether there are remote elastic support device and elastic support device or not, it is not important to the decrease of the resultant displacement, but is indispensable for decreasing the value of von Mises stress concentration. Through actual measurement, the sinking displacement of the door is less than 5 mm, which is acceptable in the project. It is demonstrated again that the single-axis-double-pin hinged door mechanism is reliable.

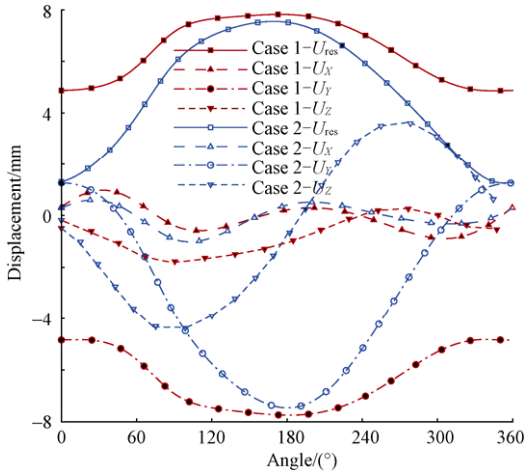

Fig. 16 Displacement curves of Cases 1-2.

5. Conclusions

1) A reliable structural design for PES vacuum chamber, which belongs to Beihang University, has been completed. The finite element method is adopted to make a static strength analysis on large-scale span reinforcing ring scheme of PES vacuum chamber and the whole chamber structure. It is demonstrated that the design of plume vacuum chamber completely meets the design requirements. The calculation result by equation is compared with the result from finite element buckling analysis. The result of eigenvalue buckling analysis is more accurate.

2) Three schemes are put forward, which resolve the problem of improper fit of the two flange faces of large side door mechanism after the door closes. After comparisons are made, the single-axis-double-pin hinged door is selected. The result of the static strength analysis for the optimal scheme shows that the structural strength of this mechanism fully meets the requirements. The maximum deformation occurs on the right side of the door flange far from the hinges. The maximum deformation is mainly caused by the deformation of *Y* direction. Whether there are a remote elastic support device and elastic support device at the bottom of hinges or not, the deformation of the door is within the permitted range, i.e., 7.8 mm. The support is not important to the decrease of the resultant displacement, but is indispensable for decreasing the value of stress concentration. The actual sinking displacement of the door mechanism is less than 5 mm. The design completely meets the requirements, thus providing a reference for the project of large hinged door mechanism.

References

[1] Ketsdever A D. An overview of ground based spacecraft-thruster interaction studies: facility design issues. AIAA-2000-0463, 2000.

[2] Lutfy F M, Vargo S E, Muntz E P. The David P. weaver collaborative high altitude flow facility's CHAFF-4 for studies of spacecraft propulsion plume contamination. AIAA-1998-3654, 1998.

[3] Dettleff G, Plahn K. Initial experimental results from the new DLR-high vacuum plume test facility STG. AIAA-1997-3297, 1997.

[4] Dettleff G, Plahn K. Experimental investigation of fully expanding free jets and plumes. Proceedings of the 21st International Symposium on Rarefied Gas Dynamics. 1999; 607-614.

[5] Dettleff G. Heat transfer measurements on a plate adjacent to a bipropellant thruster. Proceedings of the 3rd International Conference on Spacecraft Propulsion. 2000; 460-465.

[6] Ketsdever A, Jamison A, Eccles B, et al. An advanced cryogenic pumping concept for spacecraft-thruster interaction and contamination facilities. AIAA-2000-2362, 2000.

[7] Lutfy F M, Green A A, Muntz E P, et al. Investigation of the operational envelope of the CHAFF-IV plume and contamination: the mospheric flow simulator. AIAA-1999-2719, 1999.

[8] Muntz E P. Significant increase in the cryogenic pumping system capacity and reliability for the CHAFF-IV plume and contamination facility. ADA412533, 2002.

[9] Rigato W, Boldrin M, DalBello S, et al. Design, interface development and structural analyses of SPIDER vacuum vessel. Fusion Engineering and Design 2010; 85(6): 2305-2311.

[10] Ye X Z, Chen C Q. COSMOSWorks designer. Beijing:

China Machine Press, 2008; 5-20. [in Chinese]
[11] Wang S, Liu L J, Dong C M, et al. Finite element analysis theory and application with ANSYS. 3rd ed. Beijing: Publishing House of Electronics Industry, 2008; 493-501. [in Chinese]
[12] Yu W W, Gao B J. ANSYS application in the mechanical and chemical equipment. 2nd ed. Beijing: China Water Power Press, 2007; 44-183. [in Chinese]
[13] Cheng J M, Huang W, Wang L. The structure design of a diameter of 5 m manned cabin door. Environment Simulation Technology 1996; 49(4): 1-5. [in Chinese]
[14] Cai G B, Wang W L, Ling G L, et al. Quasi-hinged door. Chinese Patent Application No.200910088129.1, 2009. [in Chinese]
[15] Cai G B, Wang W L, Ling G L, et al. Double-cylinder hinged door. Chinese Patent Application No.200910088129.1, 2009. [in Chinese]
[16] Cai G B, Wang W L, Ling G L, et al. Single-axis-double-pins hinged door. Chinese Patent Application No.200910088129.1, 2009. [in Chinese]
[17] Wang W L, Ling G L, Cai G B. Deformation simulation of single-axis double-pin hinged doors. Chinese Journal of Vacuum Science and Technology 2011; 31(1): 50-56. [in Chinese]
[18] Huang B C, Cheng J M, Qi Y, et al. Vacuum chamber design. Chinese Space Science and Technology 2002; 6(3): 6-12. [in Chinese]
[19] Huang B C, Cheng J M. Space vacuum environment and vacuum technology. Beijing: National Defense Industry Press, 2005; 24-27. [in Chinese]
[20] Cheng D X. Handbook of mechanical design. Beijing: Chemical Industry Press, 2009; 7_395-7_403. [in Chinese]
[21] Pu G Y. An basic course and examples of ANSYS Workbench 12. Beijing: China Water Power Press, 2007; 178-193. [in Chinese]

Biographies:

WANG Wenlong is a Ph.D. student at School of Astronautics, Beihang University. He received his B.S. degree from Beihang University in 2006. His main research interest is on key technologies of vacuum plume effects experimental system and plume experimental study.
E-mail: wangwenlong@sa.buaa.edu.cn

CAI Guobiao is a professor and Ph.D. supervisor at School of Astronautics, Beihang University. He received the Ph.D. degree from the same university in 1996. His research interests include the vacuum plume effects and control technology, the rocket engine optimization and simulation techniques, the rocket engine re-use technology and hybrid rocket engine technology and application.
E-mail: cgb@buaa.edu.cn

ZHOU Jianping is a professor and Ph.D. supervisor at School of Astronautics, Beihang University. He received the Ph.D. degree from National University of Defense Technology in 1989. Now he is the chief designer of China Manned Space Engineering Project.
E-mail: lalzjp@vip.sina.com.cn